ADVANCED MATERIALS
www.advmat.de

A Microfluidic Ion Pump for In Vivo Drug Delivery

Ilke Uguz, Christopher M. Proctor, Vincenzo F. Curto, Anna-Maria Pappa, Mary J. Donahue, Magali Ferro, Róisín M. Owens, Dion Khodagholy, Sahika Inal, and George G. Malliaras**

Implantable devices offer an alternative to systemic delivery of drugs for the treatment of neurological disorders. A microfluidic ion pump (μFIP), capable of delivering a drug without the solvent through electrophoresis, is developed. The device is characterized in vitro by delivering γ-amino butyric acid to a target solution, and demonstrates low-voltage operation, high drug-delivery capacity, and high ON/OFF ratio. It is also demonstrated that the device is suitable for cortical delivery in vivo by manipulating the local ion concentration in an animal model and altering neural behavior. These results show that μFIPs represent a significant step forward toward the development of implantable drug-delivery systems.

Neurological disorders, ranging from emotional disorders, such as clinical depression, to chronic movement disorders such as Parkinson's disease, represent a major health concern worldwide. They strike millions of people each year, accounting for an annual economic cost of hundreds of millions of dollars that include not only direct expenses such as hospitalization and prolonged care, but also indirect ones caused by subsequent productivity losses.[1,2] The most common method to treat nervous-system disorders is oral or intravenous administration of pharmaceutically active compounds. These methods, however, require repeated administration to keep the drug concentration within the therapeutic window. Moreover, such methods allow drugs to diffuse over the whole body and interact with tissues indiscriminately. Drug delivery in the brain is often precluded by a variety of physiological and metabolic obstacles such as the blood–brain barrier (BBB).[3–5] This necessitates a higher dosage of drug to be administered, which can have detrimental effects on healthy organs and tissues that are not involved in the pathological activity.[6] It is, therefore, an ongoing target of the biomedical community to pursue novel administration strategies for efficient delivery of drugs to the central nervous system with greater precision and fewer side effects than conventional methods. Therapeutic strategies that control drug release spatially and temporally will thus have significant clinical impact.

Implantable drug-delivery devices offer an alternative to systemic administration, with the obvious advantage of localized release. One example is convection-enhanced delivery (CED) devices, which are based on drug infusion under high pressure using an intracranial needle or a catheter.[7] Direct infusion of the drug to the target site bypasses the BBB and allows for high local concentrations without side effects that would otherwise occur during systemic delivery.[8] CED systems are further improved by integrating microfluidics, which enable automated and on demand transport of small aliquots of drug molecules.[9,10] These systems, initially validated in in vitro platforms, can also be implanted as they are integrated with soft and flexible substrates such as poly(dimethylsiloxane) (PDMS) and parylene.[11–13] However, fluid-delivery systems have their shortcomings: the fluid delivered alongside the drug molecules increases local pressure around the target area, which can alter the biological properties of adjacent neural networks.[14] Moreover, accurate control of delivery and avoidance of backflow require the inclusion of valves and actuators, which complicate device fabrication and operation.[15]

An alternative therapeutic platform that addresses these issues is the organic electronic ion pump (OEIP).[16,17] Ion pumps rely on electrophoresis to transport ions from a source solution to a target solution through a polyelectrolyte film, i.e., an "ion bridge." The delivery is "dry," meaning that only the drug and not the solvent is delivered, which avoids local pressure buildup at the delivery point. Transport of ions in the opposite direction (from target to source) is blocked due to the selectivity of the polyelectrolyte (i.e., polyanion films selectively transport cations) and the directionality of the applied voltage.[18] Finally, through microfabrication, OEIPs deliver drugs with exquisite spatiotemporal control.[19] These devices were shown to control signaling in individual cells in a culture by means of K^+ delivery,[16] and to control epileptiform activity in a tissue slice model by delivery of γ-amino butyric acid

Dr. I. Uguz, Dr. C. M. Proctor, Dr. V. F. Curto, A.-M. Pappa, Dr. M. J. Donahue, M. Ferro, Prof. R. M. Owens, Prof. G. G. Malliaras
Department of Bioelectronics
Ecole Nationale Supérieure des Mines
CMP-EMSE, MOC, 13541 Gardanne, France
E-mail: malliaras@emse.fr
Prof. D. Khodagholy
Department of Electrical Engineering
Columbia University
NY 10027, USA
Prof. S. Inal
Biological and Environmental Science and Engineering
King Abdullah University of Science and Technology (KAUST)
Thuwal 23955-6900, Kingdom of Saudi Arabia
E-mail: sahika.inal@kaust.edu.sa
The ORCID identification number(s) for the author(s) of this article can be found under http://dx.doi.org/10.1002/adma.201701217.

DOI: 10.1002/adma.201701217

(GABA).[20,21] OEIPs were also used in vivo, to control hearing in a guinea pig model by delivery of acetylcholine,[17] and to control neuropathic pain in a rat model by delivery of GABA.[22]

The main limitation of the OEIP is the high voltage that is required for its operation. Indeed, in a typical in vivo application, the ion bridge that connects the source reservoir outside the body to the target inside the body is centimeter long. Owing to low drift mobility of ions in polyelectrolytes, voltages of tens of volts are typically required to deliver drug amounts that are within the therapeutic window. These values are too high for in vivo applications, as they carry the risk of electrolysis. In this paper, we address this limitation by designing a microfluidic ion pump (μFIP). Namely, we use a microfluidic system to bring the drug molecules close to the delivery point, where they can be electrophoretically pumped outward to the target through small holes coated with an ion bridge material. The concept of the μFIP and the fabrication process are shown in **Figure 1**. The device consists of two parylene sheets that are sandwiched with double-sided adhesive tape to form a microfluidic channel. The top sheet contains an area with through-holes coated with the ion bridge material, and surrounded by a horseshoe-shaped poly(3,4-ethylenedioxythiophene):polystyrene sulfonate (PEDOT:PSS) electrode that provides electrical contact to the target solution located outside the microfluidic channel. The bottom sheet contains a PEDOT:PSS electrode that establishes electrical contact to the source solution located inside the microfluidic channel. Medical-grade, double-sided adhesive tape holds the two parylene sheets together, defining a linear microfluidic channel with a length of 5.5 cm between the inlet and the outlet ends, with the ion pump located in the middle of the device. The microfluidic channel has a height of 80 μm and a width varying from 1 mm at the center, to 6 mm at the inlet and outlet ends. The top and bottom parylene sheets have a thickness of 3.5 and 3 μm, respectively, yielding a structure that is mechanically flexible. The details of the fabrication process are provided in the Experimental Section.

Figure 2 shows 16 through-holes coated with the ion bridge material. The through-holes have a nominal diameter of ≈15 μm and are distributed over an area of 200 μm × 200 μm at the center of the device. The ion bridge is made by chemically bleaching PEDOT:PSS, which destroys the π-conjugation of the PEDOT phase, and disrupts electronic transport.[23] Cationic transport in the PSS phase, however, is maintained, and when an appropriate voltage is applied between the electrodes inside and outside of the microfluidic channel, cations from the source solution are pumped outward to the target solution. An ion bridge with a nominal thickness of 6 μm (Figure 2) provides good coverage of the through-holes, blocking the transport of fluid between source and target. We find that small through-holes with a large spacing between them enable the deposition of a homogenous layer of the ion bridge material with thickness larger than 4 μm. Thinner films provide poor coverage or show cracks.

The performance of the devices was first evaluated in vitro by pumping GABA, a neurotransmitter that has been used in conjunction with OEIPs to control epileptiform activity in in vitro models.[20,21] The microfluidic channel was filled with a GABA source solution (0.05 M in deionized (DI) water) with a pH of 6.5 corresponding to 0.5×10^{-3} M $GABA^+$ ions.[24] A buffer (1 × PBS) was used as the target. The electrode outside

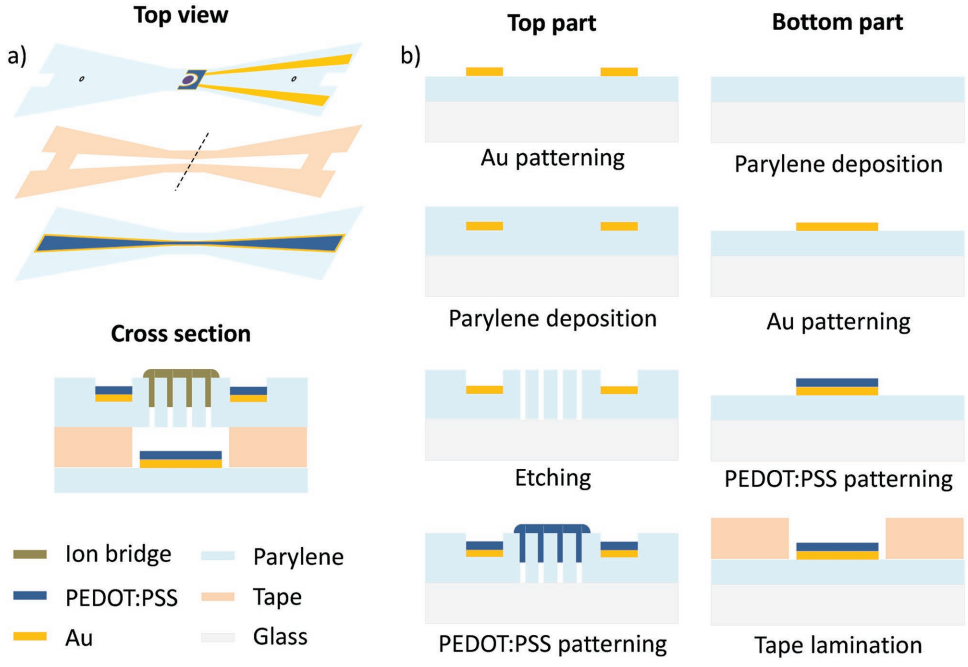

Figure 1. Schematics of the general device structure and the associated fabrication process (not to scale). a) Exploded view showing the three components with the top part of the device containing the ion bridge at the center, the horseshoe-shaped PEDOT:PSS electrode with its Au interconnects, and the inlet and outlet holes of the microfluidic; the double-sided adhesive tape that defines the microfluidic channel; and the bottom part of the device with the PEDOT:PSS electrode making contact with the source solution. The dashed line indicates the location of the cross-section shown below. b) Fabrication process for the top and bottom parts of the device.

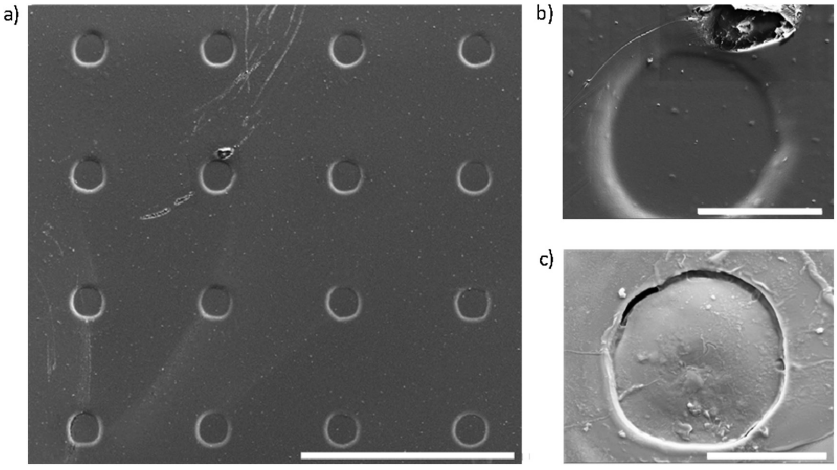

Figure 2. Scanning electron microscopy (SEM) images of through-holes coated with the ion bridge layer. a) Top-side view of the whole array of 16 through-holes, 100 µm scale bar; b) top-side view of a through-hole, showing a continuous film despite the presence of an asperity at the edge, 10 µm scale bar; c) underside view of a through-hole, 10 µm scale bar.

the microfluidic channel was grounded and a voltage of 0.5 V was applied to the electrode inside the channel. The device was operated for a period of t = 150 s, and the total amount of GABA, GABA(t), in the target was determined using a colorimetric assay, as described in the Experimental Section. At the same time, the current flowing through the device was measured and integrated to yield charge, $Q(t)$. We defined the pumping efficiency η as the fraction of charge that is carried by GABA, $\eta = F \times \text{GABA}(t)/Q(t)$, where F = 96 485 C mol^{-1} is the Faraday constant. After this calibration step, the solutions were renewed and the experiment was repeated for different applied voltages and for devices with ion bridges of different thickness. The amount of GABA delivered in 1 s was calculated as GABA(1 s) = $\eta \times Q(1\text{ s})/F$. **Figure 3** shows the amount of GABA delivered from a device with a 6 µm thick ion bridge as a function of applied bias. We find that, in this case, GABA accounted for 91% of the charge measured (η = 0.91), meaning that the vast majority of ions pumped correspond to the neurotransmitter. The high efficiency shows that the selectivity of the ion bridge to cations is indeed high, as is typically found in ion-exchange membranes used for electrodialysis.[18] The small discrepancy between estimated and measured concentrations is due to trace amounts of other cations in the source reservoir and ion bridge, as well as the transport of co-ions in the reverse direction. Assuming that the electrophoretic current is dominated by the ionic resistance of the ion bridge, the amount of GABA delivered is proportional to the applied bias (see Equation S7 in the Supporting Information). Indeed, a linear equation with an intercept of zero gives a good fit to the data for a 6 µm thick ion bridge, yielding a slope of 0.7 nmol V^{-1}. Taking the density of GABA in the ion bridge to be equal to the density of sulfonate anions,[25] the mobility of GABA in the ion bridge is estimated to be $\approx 5 \times 10^{-5}$ cm^2 V^{-1} s^{-1}. This is about four times less than the mobility of GABA in water,[26] consistent with previous findings for similarly sized ions in PEDOT:PSS.[27]

Data from a device with no ion bridge (0 µm) are also shown in Figure 3 for comparison. The pumping efficiency was low (η = 0.02) in this case, showing that in the absence of selectivity endowed by the ion bridge, the anionic current from the target to the source dominates the current (the concentration of anions in the target side is ≈200 times that of GABA$^+$ in the source solution). Data from devices with ion bridges of 3 and 4.5 µm nominal thickness fall between the two curves of Figure 3 (not shown here), indicating that ion bridge thickness and applied bias can be used to control the amount of drug delivered. The pumping efficiencies for these two devices were η = 0.75 and 0.95, respectively, consistent with the fact that 3 µm thick ion bridges showed a few cracks. The inset shows the amount of GABA delivered at an applied bias of 0.5 V for devices with different ion bridge thickness. The line is a fit to Equation S7 in the Supporting Information, showing the behavior expected from the ionic resistor model.

At zero applied bias there is no electrophoresis, but some drug is still being delivered due to diffusion. Ideally, this amount should be as low as possible in order to avoid constant exposure of tissues to the drug. Using the colorimetric GABA assay, we found these amounts to be low. As seen in Figure 3, the amount of GABA delivered by diffusion is several orders of magnitude lower than the amount delivered during electrophoresis. Moreover, diffusive delivery can be controlled by the thickness of the ion bridge. Compared to the case of open through-holes, Figure 3 shows that a 6 µm thick ion bridge causes a reduction of the amount of GABA delivered by almost two orders of magnitude. The amount of GABA delivered in the latter case is 10^{-5} nmol corresponding to a diffusion

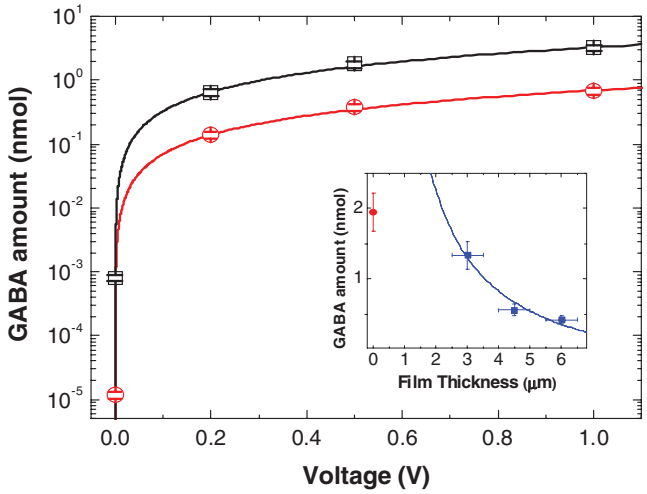

Figure 3. Amount of GABA delivered to the target in 1 s as a function of applied bias for a device with a 6 µm thick ion bridge (red circles) and a device with no ion bridge (black squares). The error bars represent the accuracy of the GABA assay. The lines are fits to a linear equation with zero intercept. The inset shows the amount of GABA delivered as a function of ion bridge thickness at an applied bias of 0.5 V. The error bars represent the accuracy of the GABA assay and the uncertainty in the thickness of the ion bridge. The line is a fit to the model (data point corresponding to 0 µm not included in the fit).

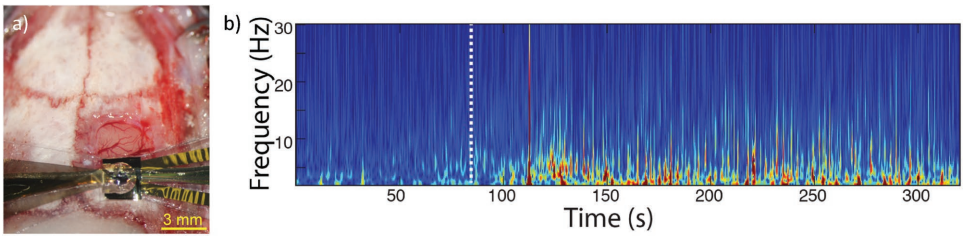

Figure 4. a) Photograph showing the μFIP placed onto the surface of the cortex. b) Intensity of spiking activity over time. The dotted line shows the moment the device is turned on by applying 0.5 V.

flux of 6×10^{-7} nmol s^{-1} per through-hole. Such a small diffusion flux is typical of ion-exchange membranes as cations ($GABA^+$) diffuse across the ion bridge with their co-ion (OH^-) and the concentration of co-ions in the ion bridge is limited by Donnan exclusion.[18]

To understand the diffusion rate in the context of biology, we follow the approach of Williamson et al.[20] Taking the volume of a half-sphere centered on a single through-hole with a radius equal to the diffusion length of GABA in water, this corresponds to a local concentration of roughly 0.6×10^{-6} M after 30 s of passive diffusion. Even ignoring the existence of powerful uptake mechanisms that would actively reduce the local GABA concentration in biological media, this is well below the extracellular GABA concentration previously demonstrated to inhibit neuronal activity, typically between 7×10^{-6} and 20×10^{-6} M.[28]

The results above show that the μFIP offers dramatically better performance than traditional OEIPs. First, the operation voltage is dramatically reduced to values below the threshold of electrolysis. Second, a large amount of drug can be delivered. For example, for the device with the 6 μm ion bridge, the application of 1 V for 1 s results in the delivery of 0.7 nmol of GABA. This amount can be further increased by increasing the number of through-holes. Normalizing by outlet area, this represents a nearly 20-fold increase in the active pumping flux for GABA at only 1/20th of the voltage compared to previous reports of traditional OEIPs.[20] Finally, the ON/OFF ratio of these devices is exceptionally high. For example, the device with the 6 μm thick ion bridge shows an ON/OFF ratio between 1 and 0 V of nearly five orders of magnitude. Previous OEIPs reported ON/OFF ratios of three orders of magnitude using a source reservoir of 100×10^{-3} M KCl.[16] The improved ON/OFF ratio reported here can largely be attributed to the decrease in the source concentration of the diffusing cation (0.5×10^{-3} vs 100×10^{-3} M) which directly limits the diffusion flux.

The successful transport of GABA encouraged us to evaluate the device in vivo. The purpose of this experiment is to demonstrate that the pump is consistent with in vivo applications, and we used a simple model to show that the pump can alter neural behavior by manipulating the local ion concentration. Owing to the mechanical flexibility and biocompatible encapsulation (parylene) of the device, we were able to place and maintain the device on the surface of the cortex without applying any force (**Figure 4**). We filled the reservoir microfluidics with KCl solution in order to deliver potassium ions which are known to induce hyperexcitability. A craniotomy (3 mm × 3 mm) was performed over the cortex and the device was laid over the surface of the brain. A tungsten multielectrode array electrode was implanted next to the active area of the pump to monitor neural activity in the cortex. The data show that activation of the pump, at the moment indicated by the dashed line, results to the emergence of hyperexcitability as a result of K^+ increase (Figure 4b). The activity starts in only a matter of seconds, demonstrating that the μFIP is compatible with in vivo drug delivery.

Here, we have used the microfluidic channel as a passive drug reservoir. Future work will explore continuous flow in the microfluidic channel as a way to dynamically switch the drug being delivered. For fully implanted applications, the channel can be connected with a subcutaneous reservoir that is refilled with a syringe, as practiced in some convection-enhanced delivery systems. Moreover, the addition of microelectrodes for electrical recording/stimulation can be achieved in a straightforward manner (during the deposition of the top PEDOT:PSS electrode), paving the way for multimodal, closed-loop systems. Simple variations of architecture can enable forms that penetrate the brain with the aid of a sacrificial shuttle,[29] suitable for localized drug delivery past the blood–brain barrier. Such an implantable probe incorporating a μFIP could be a promising alternative to CED due to the inherently dry delivery of ion pumps. Other applications, such as the subcutaneous delivery of insulin for diabetics, can also be targeted using a μFIP with appropriate ion bridge materials. In addition to therapeutic applications, the finely tuned spatial and temporal control of ion delivery offered by the μFIP may prove to be a valuable tool for fundamental research in biology. Finally, by replacing the ion bridge with a micro-/nanoporous membrane, the device could also be adapted to microdialysis applications.

In conclusion, we have developed a microfluidic ion pump suitable for in vivo drug delivery. The purpose of the microfluidic is to bring the drug as close to the delivery point as possible, thereby minimizing the path length for transport within the ion bridge. The μFIP shows dramatically improved performance compared to traditional ion pumps, offering low-voltage operation, high delivery capacity, and high ON/OFF ratio. These improvements represent a significant step forward toward the development of implantable drug-delivery systems.

Experimental Section

Fabrication of the Devices: Glass sides with dimensions of 1 in. × 3 in. were cleaned by sonication, first in 2 vol% soap solution in water, then in acetone. For the fabrication of the top part of the device (Figure 1), a 1.7 μm thick parylene-C film was deposited using an SCS Labcoater 2. An S1813 (Shipley) photoresist was spin cast and exposed to UV light using

a SUSS MJB4 contact aligner, with the mask designed for patterning the Au interconnects. The resist was then developed with MF-26A developer. A 10 nm thick layer of Cr was deposited followed by the deposition of a 100 nm thick Au layer (Alliance Concept EVA450). The patterning of the interconnects was finalized by lift-off in acetone. A second 1.8 µm parylene film was then deposited, after treating the structure with a silane as an adhesion promoter. AZ9260 was subsequently spin coated, exposed, and developed using AZ developer, followed by reactive ion etching (Oxford 80 plus plasma etcher) to obtain the outline of the top part of the device. A third (sacrificial) layer of parylene was deposited on this structure using 2 vol% soap solution to minimize adhesion. AZ9260 photoresist was deposited, exposed using a mask for defining the outline of the ion bridge pattern, and the etching of the sacrificial layer of parylene film was performed. A second AZ9260 was deposited and exposed to open the through-holes and areas for PEDOT:PSS deposition. The devices used for the in vitro characterization had 16 through-holes, while the in vivo version of the device had 300 through-holes. After etching, an aqueous dispersion of PEDOT:PSS (PH 1000 from H.C. Stark) containing 5 vol% of ethylene glycol, 0.1 vol% dodecyl benzene sulfonic acid, and 1 wt% of (3-glycidyloxypropyl) trimethoxysilane (GOPS) was spin cast on the substrates. Multiple depositions were used to control the thickness, with a 1 min long of soft baking step at 110 °C following each deposition. Finally, the sacrificial third layer of parylene was peeled off to complete the patterning of PEDOT:PSS. Subsequent to hard baking at 140 °C, the top part was peeled from glass and placed upside down on a glass slide. A drop of bleach was placed on the film for 30 s to induce overoxidation of the PEDOT:PSS film in the through-holes. The thickness of the ion bridge was measured outside the through-holes using a Dektak mechanical profilometer. The thickness inside the through-holes was estimated by assuming complete filling, i.e., adding the thickness of the parylene film to the measured thickness of the ion bridge. For the fabrication of the bottom part of the device (Figure 1), a layer of parylene (≈3 µm) was coated on a glass slide. Cr/Au and PEDOT:PSS patterning on this film was performed using the same protocol applied for the top part. For the in vitro tests, the devices had a glass slide instead of a bottom parylene sheet. The top and bottom parts were stuck together with the help of 80 µm medical-grade double adhesive tape (1500 transparent polyethylene, 3M), cut to the shape of the fluidic channel using a flatbed plotter (FC2250, Graphtec).

Quantification of GABA in the Target Electrolyte: The microfluidic channel was filled with a GABA source solution (0.05 M in DI water), and a buffer (1 × PBS) was used as the target. A PDMS reservoir, with a volume capacity of 100 µL, was used to contain the target solution. A voltage was applied and the device was run for 150 s, while the current was measured. A Keithley 2612A SourceMeter unit with customized labview software was used to drive the devices. The target solution was then collected, and the target reservoir was rinsed with 20 µL of deionized water that was subsequently added to the collected target solution to ensure that most of the GABA was collected. The concentration of GABA was then measured using a GABA Assay Kit (ImmuSmol) according to manufacturer's instructions. For the diffusion measurements, we ensured that the ion bridge was fully filled with GABA cations by operating the device at 0.5V. The target solution (PBS) was then placed and the diffusion measurements started. To account for the low amount of GABA, the measurement time was 1000 s.

In Vivo Validation: All the animal experiments were approved by the Institutional Animal Care and Use Committee. One male Long Evans rat (280 g; 10 weeks of age) was housed in a regular 12/12 h light/dark cycle throughout the course of experimentation. It was initially anesthetized with 2% isoflurane and maintained under anesthesia with 0.75–1% isoflurane during the surgery and intraoperative recordings. A 3 mm × 3 mm craniotomy was performed on the right hemisphere (anterior–posterior (AP) = 3.5 mm, medial–lateral (ML) = 3 mm) and the µFIP was placed on the exposed cortical surface. A four-wire 50 µm tungsten multielectrode array was inserted in the brain in the neighborhood of the µFIP and was used to record brain activity. Two tungsten wires with 100 µm diameter and 2 mm length were implanted in cerebellum to serve as ground and reference electrodes.

Supporting Information

Supporting Information is available from the Wiley Online Library or from the author.

Acknowledgements

I.U. and C.M.P. contributed equally to this work. Financial support from the Région PACA, the Whitaker Foundation, and the Fondation pour la Recherche Médicale (FRM DBS20131128446) is acknowledged. I.U. thanks Microvitae for supporting the bourse Région.

Conflict of Interest

The authors declare no conflict of interest.

Keywords

organic bioelectronics, organic electronic ion pumps, PEDOT:PSS

Received: March 2, 2017
Revised: March 25, 2017
Published online: May 15, 2017

[1] WHO—Neurological Disorders: Public Health Challenges, http://www.who.int/mental_health/neurology/neurodiso/en/(accessed: December 2016).
[2] A. Gustavsson, M. Svensson, F. Jacobi, C. Allgulander, J. Alonso, E. Beghi, R. Dodel, M. Ekman, C. Faravelli, L. Fratiglioni, B. Gannon, D. H. Jones, P. Jennum, A. Jordanova, L. Jönsson, K. Karampampa, M. Knapp, G. Kobelt, T. Kurth, R. Lieb, M. Linde, C. Ljungcrantz, A. Maercker, B. Melin, M. Moscarelli, A. Musayev, F. Norwood, M. Preisig, M. Pugliatti, J. Rehm, L. Salvador-Carulla, B. Schlehofer, R. Simon, H.-C. Steinhausen, L. J. Stovner, J.-M. Vallat, P. Van den Bergh, P. V. den Bergh, J. van Os, P. Vos, W. Xu, H.-U. Wittchen, B. Jönsson, J. Olesen, CDBE2010 Study Group, *Eur. Neuropsychopharmacol.* **2011**, *21*, 718.
[3] W. M. Scheld, *Rev. Infect. Dis.* **1989**, *11*, S1669.
[4] W. Löscher, H. Potschka, *Nat. Rev. Neurosci.* **2005**, *6*, 591.
[5] C. F. Higgins, *Nature* **2007**, *446*, 749.
[6] V. P. Torchilin, *Eur. J. Pharm. Sci.* **2000**, *11*, S81.
[7] R. H. Bobo, D. W. Laske, A. Akbasak, P. F. Morrison, R. L. Dedrick, E. H. Oldfield, *Proc. Natl. Acad. Sci. USA* **1994**, *91*, 2076.
[8] O. Lewis, M. Woolley, D. Johnson, A. Rosser, N. U. Barua, A. S. Bienemann, S. S. Gill, S. Evans, *J. Neurosci. Methods* **2016**, *259*, 47.
[9] I. U. Khan, C. A. Serra, N. Anton, T. Vandamme, *J. Controlled Release* **2013**, *172*, 1065.
[10] R. Riahi, A. Tamayol, S. A. M. Shaegh, A. M. Ghaemmaghami, M. R. Dokmeci, A. Khademhosseini, *Curr. Opin. Chem. Eng.* **2015**, *7*, 101.
[11] J. M. K. Ng, I. Gitlin, A. D. Stroock, G. M. Whitesides, *Electrophoresis* **2002**, *23*, 3461.
[12] W. Gu, X. Zhu, N. Futai, B. S. Cho, S. Takayama, *Proc. Natl. Acad. Sci. USA* **2004**, *101*, 15861.
[13] C. P. Foley, N. Nishimura, K. B. Neeves, C. B. Schaffer, W. L. Olbricht, *Biomed. Microdevices* **2009**, *11*, 915.
[14] H. Suzuki, R. Yoneyama, *Sens. Actuators, B* **2003**, *96*, 38.
[15] C. S. Chen, J. Tan, J. Tien, *Annu. Rev. Biomed. Eng.* **2004**, *6*, 275.
[16] J. Isaksson, P. Kjall, D. Nilsson, N. D. Robinson, M. Berggren, A. Richter-Dahlfors, *Nat. Mater.* **2007**, *6*, 673.

[17] D. T. Simon, S. Kurup, K. C. Larsson, R. Hori, K. Tybrandt, M. Goiny, E. H. Jager, M. Berggren, B. Canlon, A. Richter-Dahlfors, *Nat. Mater.* **2009**, *8*, 742.
[18] Y. Tanaka, in *Ion Exchange Membranes*, 2nd ed., Elsevier, Amsterdam, The Netherlands **2015**, pp. 29–65.
[19] A. Jonsson, T. A. Sjöström, K. Tybrandt, M. Berggren, D. T. Simon, *Sci. Adv.* **2016**, *2*, e1601340.
[20] A. Williamson, J. Rivnay, L. Kergoat, A. Jonsson, S. Inal, I. Uguz, M. Ferro, A. Ivanov, T. A. Sjöström, D. T. Simon, M. Berggren, G. G. Malliaras, C. Bernard, *Adv. Mater.* **2015**, *27*, 3138.
[21] A. Jonsson, S. Inal, I. Uguz, A. J. Williamson, L. Kergoat, J. Rivnay, D. Khodagholy, M. Berggren, C. Bernard, G. G. Malliaras, D. T. Simon, *Proc. Natl. Acad. Sci. USA* **2016**, *113*, 9440.
[22] A. Jonsson, Z. Song, D. Nilsson, B. A. Meyerson, D. T. Simon, B. Linderoth, M. Berggren, *Sci. Adv.* **2015**, *1*, e1500039.
[23] P. Tehrani, N. D. Robinson, T. Kugler, T. Remonen, L.-O. Hennerdal, J. Häll, A. Malmström, L. Leenders, M. Berggren, *Smart Mater. Struct.* **2005**, *14*, N21.
[24] Chemicalize—Instant Cheminformatics Solutions, https://chemicalize.com/welcome (accessed:December 2016).
[25] C. M. Proctor, J. Rivnay, G. G. Malliaras, *J. Polym. Sci., Part B: Polym. Phys.* **2016**, *54*, 1433.
[26] M. V. Jones, P. Jonas, Y. Sahara, G. L. Westbrook, *Biophys. J.* **2001**, *81*, 2660.
[27] E. Stavrinidou, P. Leleux, H. Rajaona, D. Khodagholy, J. Rivnay, M. Lindau, S. Sanaur, G. G. Malliaras, *Adv. Mater.* **2013**, *25*, 4488.
[28] M. V. Jones, G. L. Westbrook, *Neuron* **1995**, *15*, 181.
[29] A. Williamson, M. Ferro, P. Leleux, E. Ismailova, A. Kaszas, T. Doublet, P. Quilichini, J. Rivnay, B. Rózsa, G. Katona, C. Bernard, G. G. Malliaras, *Adv. Mater.* **2015**, *27*, 4405.

